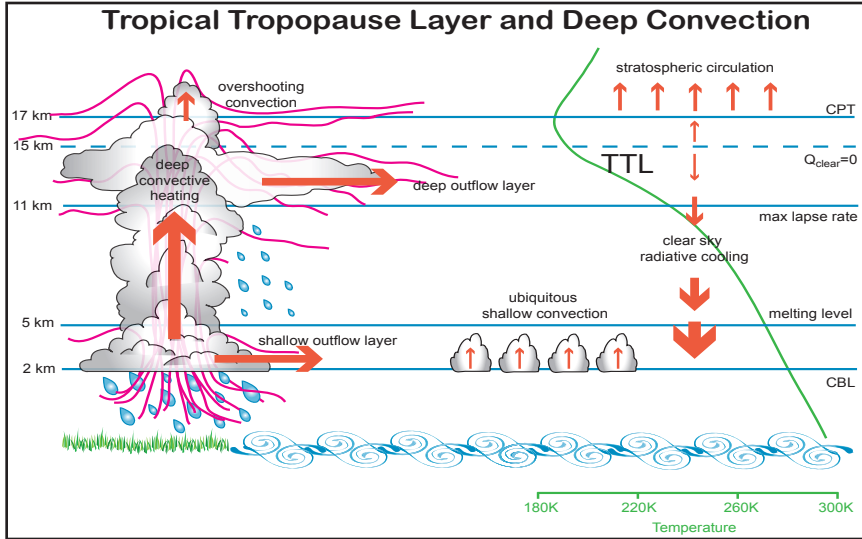


# Modelling of Deep Convection and Chemistry and their Roles in the Tropical Tropopause Layer: SPARC-GEWEX/GCSS-IGAC Workshop

June 12-15 2006, Victoria, BC, Canada



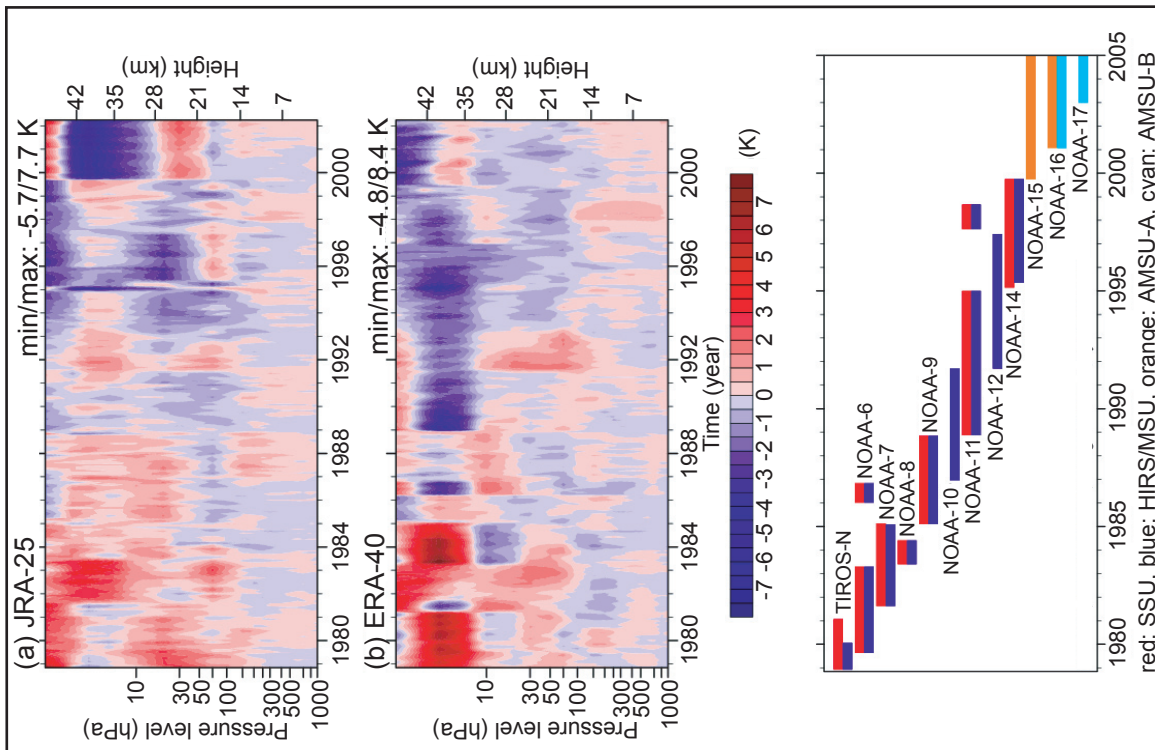
< **Figure 1**

Processes related to the TTL and deep convection in the tropics. Deep convection is shown mostly over land, where it is more common, and shallow convection over the ocean. Mass circulation is represented by the red arrows. Typical particle advection by deep convection into the TTL is shown in pink.

## Report on the SPARC Data Assimilation Workshop

2-4 October 2006, ESTEC, Noordwijk, the Netherlands

I



^ **Figure 1**

Global mean temperature anomalies of JRA-25 (upper panel) and ERA-40 (middle panel). The bottom panel is the history of vertical sounders. The original is provided by the JMA/CRIEPI cooperative reanalysis project JRA-25. (Courtesy of T. Iwasaki.)

# Report on the SPARC Data Assimilation Workshop 2-4 October 2006, ESTEC, Noordwijk, the Netherlands

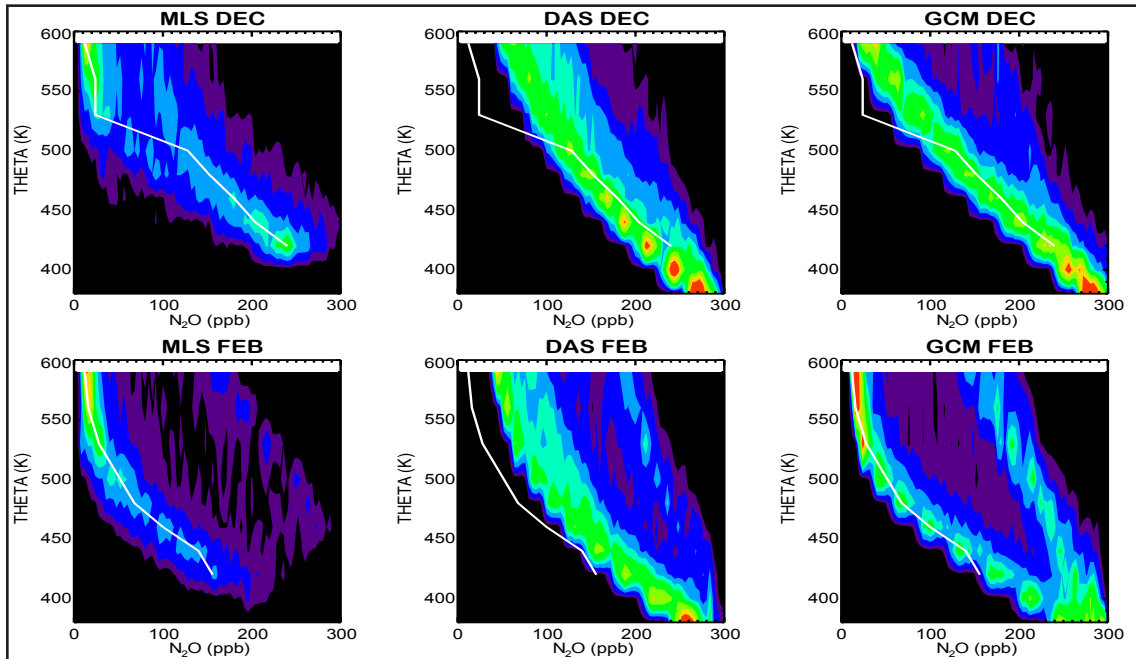


**Figure 2**

Contoured probability distribution functions (pdfs) of Aura MLS v1.5  $N_2O$  observations and simulations with the GMI Combo CTM using GEOS4 assimilated (DAS) and GEOS general circulation model (CTM) meteorological fields,  $66^{\circ}$ - $82^{\circ}$ N. Purples and blues indicate infrequently sampled mixing ratios, yellows and reds indicated the most probable mixing ratios sampled. Solid white lines represent MLS most probable profiles. (Courtesy of S. Strahan.)

II

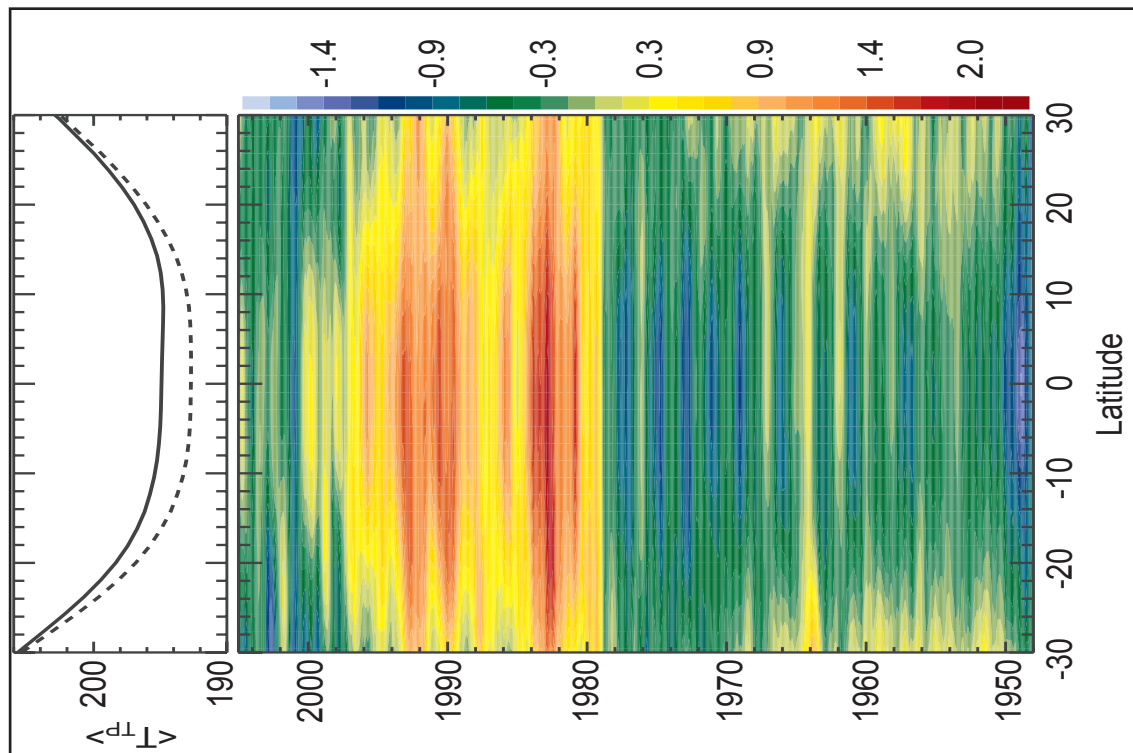
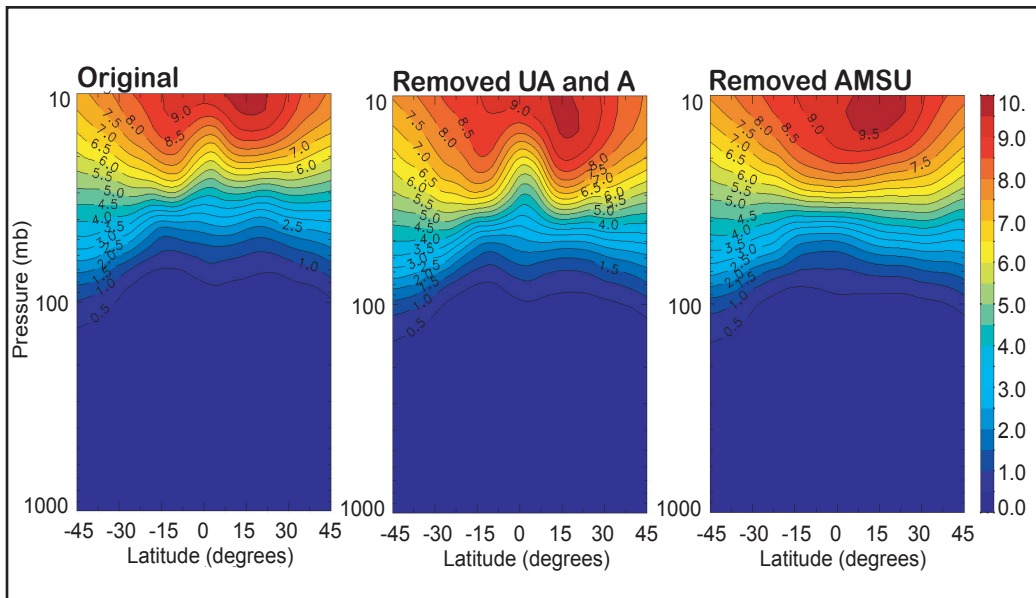


**Figure 5**

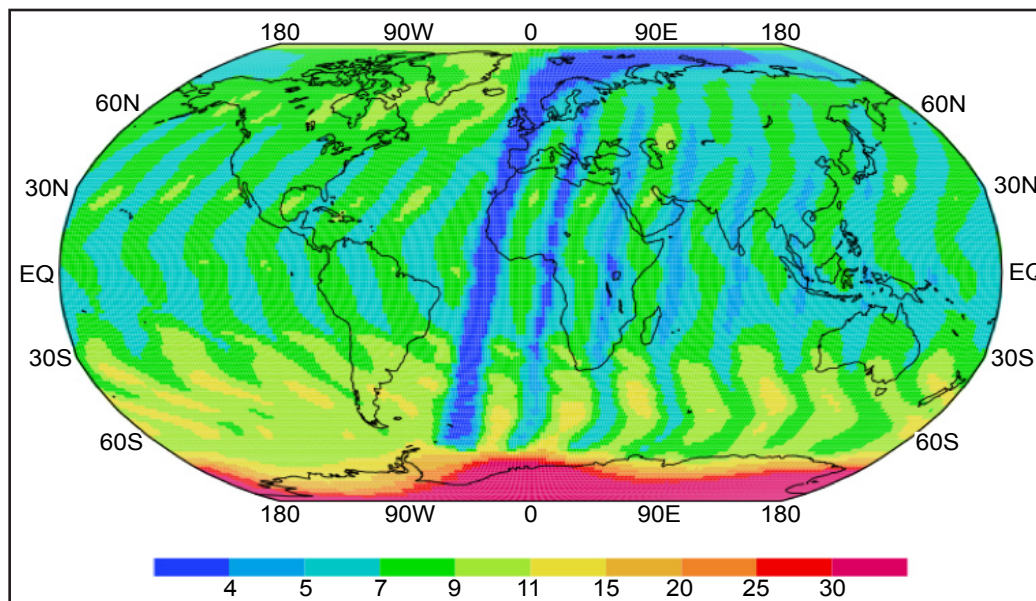
Relative deviations (in percent) of cold point temperature  $T_{cp}$  in the NCEP/NCAR reanalysis with respect to long-term monthly means. The upper panel shows the long-term mean  $T_{cp}$  as a function of latitude separated into the pre- (dashed) and post- (solid) 1979 periods (i.e. pre and post satellite era). (Courtesy of T. Birner.)



^ **Figure 10**

*GEM-Strato zonal mean ozone volume mixing ratio field (ppmv) at 00 UTC on September 6, 2003, from a 3D-Var dynamics assimilation cycle which began on August 11, 2003. The three panels show, from left to right, the ozone field subject to the transport affected by the assimilation of all observations, by the removal of radiosonde (AU) and aircraft (AI) observations, and by the removal of AMSU-A observations. The distortions show the sensitivity of the ozone field to the assimilation of AMSU-A temperature-sensitive (stratospheric) channels with unrecovered biases. The choice of background error statistics and the response of the forecast model to the assimilated temperature field also contribute to this sensitivity. (Courtesy of Y. J. Rochon.)*

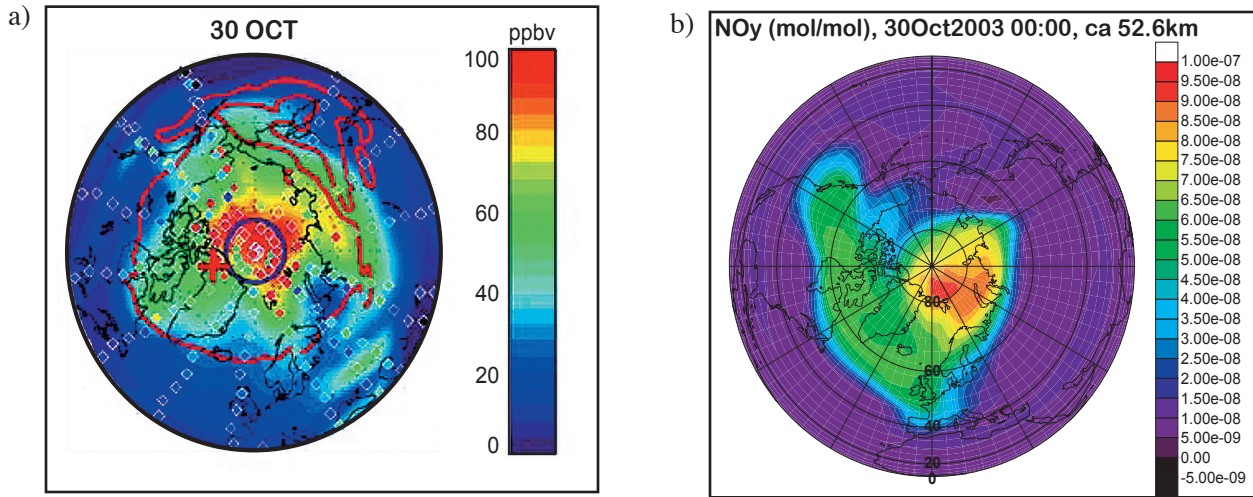
III



^ **Figure 11**

*A snapshot of the forecast error for the total column ozone, derived from the KNMI sub-optimal Kalman filter ozone assimilation system and GOME ozone column observations. The figure demonstrates several key aspects of the Kalman filter, namely (1) the forecast error is strongly reduced when new observations are added (the blue strip represents the latest GOME orbit analysed), not only at the observations but also in the surroundings (error correlation length of about 500 km), (2) the model error term causes an increase of the forecast error with time, and (3) the forecast error is a property of air parcels, and follows the atmospheric flow like ozone itself. (Courtesy of H. Eskes.)*

# Report on the first SOLARIS workshop 4-6 October 2006, Boulder, Colorado, USA

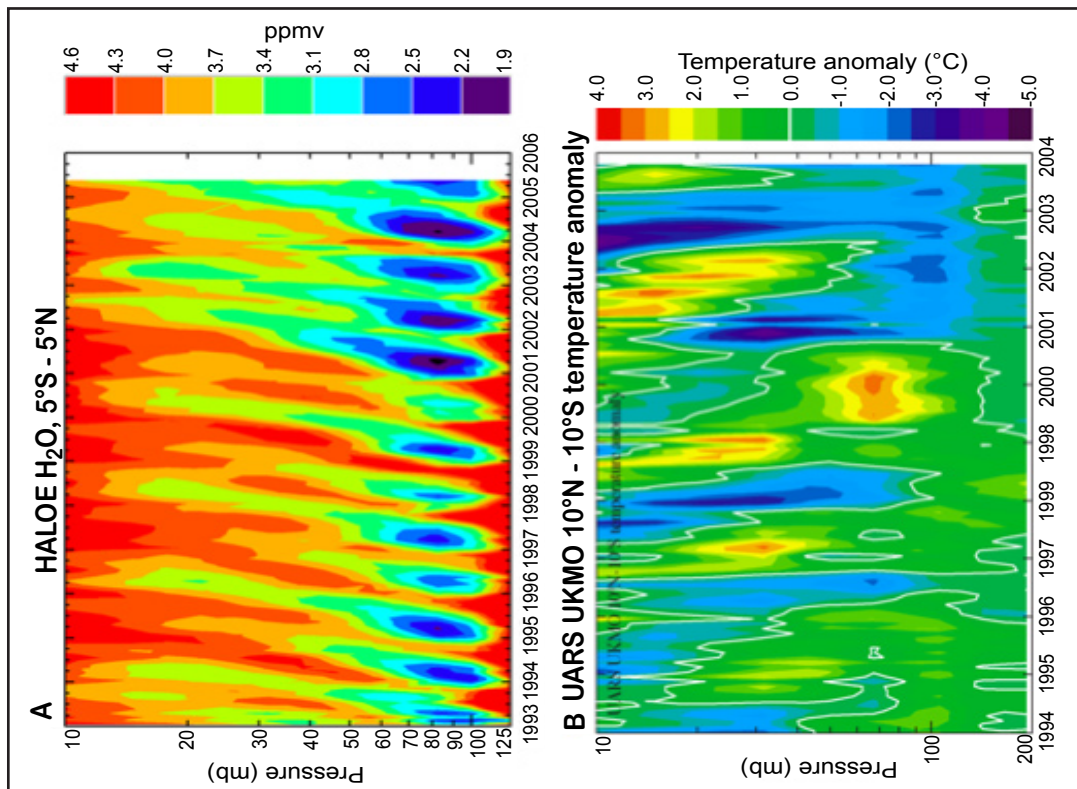


**^ Figure 1**

a)  $NO+NO_2$  (vmr) between 50-55 km from the MIPAS instrument on 30 October 2003 during a large solar proton event (From Lopez-Puertas et al., 2005); b)  $NO_y$  (vmr) at 53 km from a transient simulation with WACCM. (Courtesy of D. Marsh.)

IV

## A note on an AGU spring meeting discussion of the role of atmospheric water vapour in climate and atmospheric composition 23-26 May 2006, Baltimore, Maryland, USA



**< Figure 2**  
Evolution of the tropical (A) stratospheric water vapour from HALOE and (B) temperature from UARS.